Dual-function artificial molecular motors performing rotation and photoluminescence

Pfeifer, Lukas; Hoang, Nong V.; Crespi, Stefano; Pshenichnikov, Maxim S.; Feringa, Ben L.

Published in:
Science Advances

DOI:
10.1126/sciadv.add0410

Publication date:
2022

PHYSICS

Dual-function artificial molecular motors performing rotation and photoluminescence

Lukas Pfeifer[1]†‡, Nong V. Hoang[2]†, Stefano Crespi[1]§, Maxim S. Pshenichnikov[2]*, Ben L. Feringa[1,2]*

Molecular machines have caused one of the greatest paradigm shifts in chemistry, and by powering artificial mechanical molecular systems and enabling autonomous motion, they are expected to be at the heart of exciting new technologies. One of the biggest challenges that still needs to be addressed is designing the involved molecules to combine different orthogonally controllable functions. Here, we present a prototype of artificial molecular motors exhibiting the dual function of rotary motion and photoluminescence. Both properties are controlled by light of different wavelengths or by exploiting motors' outstanding two-photon absorption properties using low-intensity near-infrared light. This provides a noninvasive way to both locate and operate these motors in situ, essential for the application of molecular machines in complex (bio)environments.

INTRODUCTION

Artificial molecular machines—molecules designed to perform controlled, directional motion driven by external stimuli—are the basis of responsive and mechanical systems, which position them at the forefront of the chemical and materials sciences (*1*–*9*). The so-called second-generation Feringa-type motors (*10*) operate via alternating photochemical *E*/*Z* isomerization and thermal helix inversion (THI) steps of an overcrowded alkene (Fig. 1A) (*11*). A stable isomer is excited by light, which drives the population of a metastable state, from which thermal energy promotes the formation of a second stable isomer following the motor's "power stroke" (*12*). Distinct chiral elements, i.e., stereogenic center and helicity, present in the system as well as the energy difference between stable and metastable isomers (ΔG) ensure unidirectionality of the rotation (*12*, *13*).

Despite numerous seminal studies outlining potential applications of molecular motors (*13*–*17*), their use in more complex systems (e.g., biological systems) remains severely limited (*18*, *19*). Two crucial challenges need to be addressed before they can reach their full potential. First, motors driven by low-intensity, low-energy light, ideally from the near-infrared (NIR) region, are required to avoid negative side effects like limited penetration depth and photochemical side reactions related to the classically used ultraviolet (UV) light. Second, strategies to track their exact location in a noninvasive way need to be developed. A universal technique available in many biochemical laboratories, photoluminescence (PL) microscopy offers many exciting opportunities along this way (*20*, *21*). We have previously reported a molecular motor operable by low-intensity NIR light, albeit with the help of an attached second chromophore acting as NIR light–sensitive antenna (*22*). However, the design of artificial molecular motors with intrinsic PL maintaining proper motor function using NIR irradiation has so far remained unexplored, because of the formidable challenges associated with combining two light-activated functions in one molecule (*23*). An earlier example used a fluorophore attached to a molecular motor core via a long linker to break up the two functions of rotation and PL over two separate and electronically isolated parts of the molecule (*24*, *25*). In this example, rotation and PL were excited using UV and visible light, respectively.

The most elegant way to obtain a single molecule with two photostimulated functions is for them to originate from different excited states (i.e., different local minima on the surface of the same excited electronic state or two different excited electronic states) of the same chromophore, which, therefore, remains relatively compact. With rotation in overcrowded alkene-type motors normally being triggered by promotion to the S_1 state followed by relaxation through a conical intersection with the S_0 surface, PL can be achieved by either alternative, radiative relaxation from a separate, local minimum on the S_1 surface or a higher-lying excited electronic state. In both cases, relaxation via photon emission must be the fastest process available for it to be efficient, outcompeting nonradiative relaxation pathways (*26*–*28*), which is extremely challenging as evidenced by the limited number of molecules displaying this property (*29*–*35*). Nevertheless, Aprahamian and co-workers have recently reported PL from an S_n ($n \geq 2$) state in high-viscosity solvents in a series of boron difluorohydrazone dyes (*36*). However, to this date, PL has never been combined with the photochemical reactions key to the rotary motion of molecular motors in the same chromophore.

Here, we present a series of three NIR light–driven molecular motors showing intrinsic PL in addition to their motor rotation function. For two of these motors, judicious choice of wavelength or mode of excitation, one-photon excitation (1PE) versus NIR two-photon excitation (2PE), can be used to tune the selectivity between rotation and PL. The properties of the motors have been studied thoroughly using nuclear magnetic resonance (NMR), time-resolved PL spectroscopy, transient absorption (TA) spectroscopy, and time-dependent density functional theory (TD-DFT) calculations. All motors benefit from a high stability even under prolonged illumination as well as a large two-photon absorption (2PA) cross section (σ_2).

RESULTS

Figure 1B shows a conceptual potential energy diagram of our second-generation dual-function molecular motors; this diagram is based

[1]Stratingh Institute for Chemistry, University of Groningen, Nijenborgh 4, 9747 AG Groningen, Netherlands. [2]Zernike Institute for Advanced Materials, University of Groningen, Nijenborgh 4, 9747 AG Groningen, Netherlands.
*Corresponding author. Email: m.s.pchenitchnikov@rug.nl (M.S.P.); b.l.feringa@rug.nl (B.L.F.)
†These authors contributed equally to this work.
‡Present address: Laboratory of Photonics and Interfaces, Department of Chemistry and Chemical Engineering, École Polytechnique Fédérale de Lausanne, 1015 Lausanne, Switzerland.
§Present address: Department of Chemistry–Ångström Laboratory, Uppsala University, Box 523, 751 20 Uppsala, Sweden.

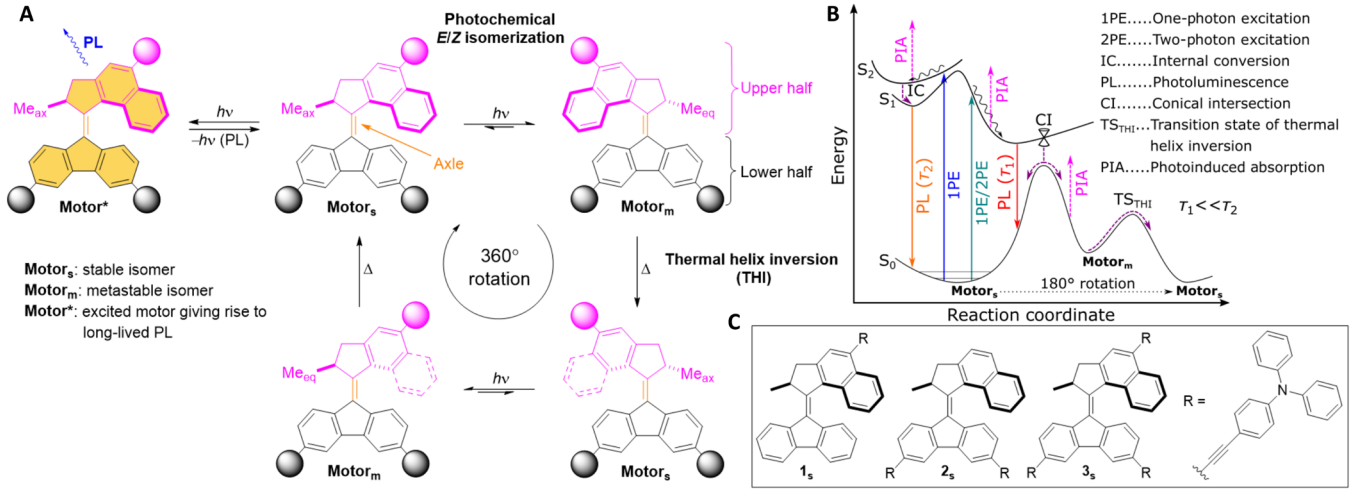

Fig. 1. Concept and compounds used in this study. (**A**) Scheme illustrating rotation and PL from a higher-lying excited-state isomer of a second-generation molecular motor. (**B**) Conceptual potential energy diagram illustrating the mode of operation of the molecular motors described in this study capable of performing rotation and undergoing relaxation via PL. (**C**) Compounds used in this study.

on the experimental results presented herein (vide infra). The right-hand part of the diagram shows typical processes of light-driven molecular motors (*37*–*39*): Excitation to the S_1 state leads to vibrational and structural relaxation from the Franck-Condon (FC) region to a conical intersection (CI) with the S_0 surface. In the productive pathway, the motor reaches a metastable isomer, which undergoes a second isomerization, i.e., a THI step to form a stable isomer (depending on the substitution pattern of the lower half of the motor, this isomer can be identical to the original stable isomer), which completes a 180° rotation. In the unproductive pathway, after passing a CI, vibrational relaxation takes the motor back to the original stable isomer. PL is realized via a separate PL pathway, originating from a putative more energetic local minimum located on the S_1 surface. This geometry is reached via initial excitation to S_2, followed by internal conversion (IC) to S_1. To prevent relaxation to the same CI with the S_0 surface giving rise to isomerization, these geometries are proposed to be separated by a potential energy barrier (*40*).

Design and fundamental properties of motors

For the design of our motors, we attached between one and three triphenylamine groups via short alkyne linkers to a central motor core (Fig. 1C). These substituents are known for increasing σ_2 of organic compounds (*41*–*43*). Because of their nitrogen lone pair, they can also act as donors in intramolecular transitions (e.g., charge-transfer transitions) potentially unlocking new photochemical reaction pathways in addition to the $\pi \rightarrow \pi^*$ transition, which initiates the rotation of these motors (*44*, *45*).

Motors $\mathbf{1_s}$ to $\mathbf{3_s}$ were prepared in three to five linear steps from commercially available materials (see section S2). When dissolved in MeCN, their lowest-energy transition peaks were centered at 438, 423, and 470 nm ($\lambda_{max,s}$; Fig. 2A), respectively, showing a substantial red shift compared to the unsubstituted motor core (R = H in Fig. 1C) due to extension of the π system (fig. S17).

Upon irradiation with light-emitting diodes (LEDs) with output wavelengths of 455 nm ($\mathbf{1_s}$), 420 nm ($\mathbf{2_s}$), and 470 nm ($\mathbf{3_s}$), these peaks undergo bathochromic shifts to 458, 448, and 496 nm (Fig. 2A), respectively, as the samples went from containing only the stable isomers to their photostationary states (PSSs), where a mixture of stable and metastable isomers is present. This behavior is characteristic for fluorene-based second-generation overcrowded alkene-type molecular motors (*46*, *47*). In all three cases, removal of the light source led to recovery of the original spectra, due to the formation of stable isomers via THI. Both photoisomerization and THI processes presented clean isosbestic points (section S5.2). These results were confirmed by ^{1}H NMR experiments [performed in dichloromethane (DCM)–d_2 due to higher solubilities] (figs. S10 to S13), from which we determined the ratios of metastable:stable isomers at the PSSs (table S1). Therefore, we concluded that compounds **1** to **3** are functional photochemically driven rotary molecular motors.

The quantum yields of photoisomerization from the stable to the metastable isomers ($\varphi_{s\rightarrow m}$) and vice versa ($\varphi_{m\rightarrow s}$) as well as the Gibbs free energies of activation ($\Delta^{\ddagger}G°$) for THI of the metastable isomers were determined, to study the influence of varying the number of triphenylamine substituents on these core parameters. As seen in Table 1, $\varphi_{s\rightarrow m}$ is about three times larger than $\varphi_{m\rightarrow s}$ in motors **1** to **3** with both decreasing upon adding more triphenylamine groups. On the other hand, $\Delta^{\ddagger}G°$ and, therefore, the half-life at 20°C increase with the addition of more substituents. By comparison, $\varphi_{s\rightarrow m}$ of the unsubstituted motor core is comparable to that of **1**, whereas its $\varphi_{m\rightarrow s}$ was reported to be about three times larger than $\varphi_{s\rightarrow m}$, making it necessary to irradiate at wavelengths with a substantial difference in absorption coefficient (ε) between the two isomers to obtain high metastable:stable ratios at PSS (*38*). $\Delta^{\ddagger}G°$ of the unsubstituted compound was lower than that of **1** (*47*), in line with the trend observed for **1** to **3**. Excellent stabilities were found for all three compounds over the course of 10 consecutive 180° rotations (insets in Fig. 2A and fig. S23) as well as 1 hour of continuous irradiation close to their respective $\lambda_{max,s}$ (fig. S25).

Motor rotation upon 2PE

Next, we examined motor function upon 2PE with 800-nm light. Steady-state absorption spectra of solution samples of $\mathbf{1_s}$, $\mathbf{2_s}$, and $\mathbf{3_s}$

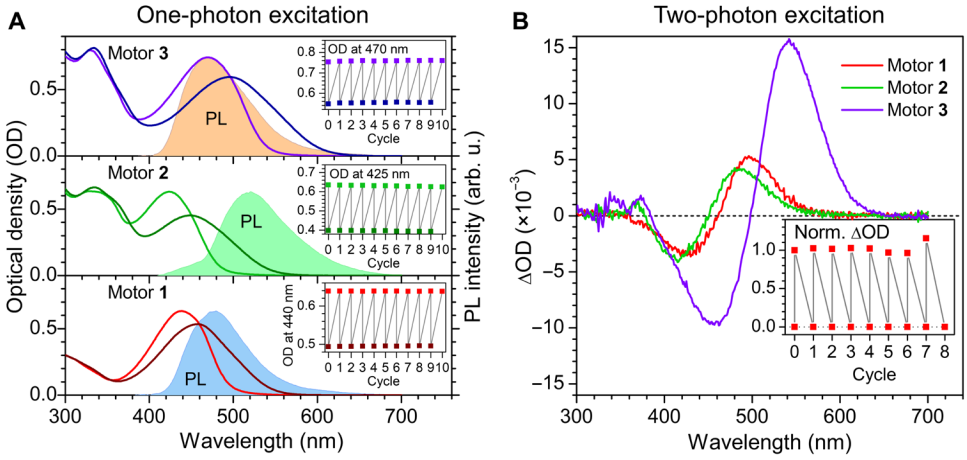

Fig. 2. Spectroscopic behavior related to rotation and PL of motors 1 to 3. (**A**) Absorption spectra of $\mathbf{1}_s$ (red), $\mathbf{2}_s$ (green), and $\mathbf{3}_s$ (violet) and the mixtures of $\mathbf{1}_s$:$\mathbf{1}_m$ (dark red), $\mathbf{2}_s$:$\mathbf{2}_m$ (dark green), and $\mathbf{3}_s$:$\mathbf{3}_m$ (dark violet) at the PSS after irradiating the samples with LEDs of an appropriate wavelength ($\mathbf{1}_s$: 455-nm LED; $\mathbf{2}_s$: 420-nm LED; $\mathbf{3}_s$: 470-nm LED) for 3 min. The insets show ODs, over 10 consecutive cycles of irradiation with identical irradiation time and light intensity, followed by relaxation of the metastable to the according stable isomers in the dark via THI. The shaded contours display steady-state PL spectra of $\mathbf{1}_s$, $\mathbf{2}_s$, and $\mathbf{3}_s$ under 400-nm excitation. (**B**) ΔOD spectra of **1** (red), **2** (green), and **3** (violet) after two-photon irradiation at 800 nm for 15 min. The peak irradiation intensity was set to 1.4 GW cm^{-2} for all compounds. The inset shows the normalized ΔOD at 500 nm of **1** over eight consecutive cycles with identical irradiation time at a light intensity of 4.5 GW cm^{-2}. Before starting a new irradiation cycle, the samples were kept in the dark for 40 to 60 min to ensure complete recovery of the stable isomer. The molar concentration of all compounds was set identical to 1.0×10^{-5} and 1.0×10^{-6} M for the measurements of the absorption and PL spectra, respectively, with MeCN as the solvent. arb. u., arbitrary units.

Table 1. Quantum yields of photoisomerization, thermodynamic activation parameters of metastable isomers, and 2PA cross sections of motors 1 to 3. Quantum yields of isomerization from the stable to the metastable isomers ($\varphi_{s\rightarrow m}$) were determined by following the formation of metastable isomers in DCM by UV-vis absorption spectroscopy using an LED with a known photon flux. From those, quantum yields for the photochemical backreaction ($\varphi_{m\rightarrow s}$) could be determined (see section S5.5). Gibbs free energies of activation ($\Delta^{\ddagger}G°$) for the formation of stable from metastable isomers by THI in MeCN were determined by Eyring analysis (section S5.3) and used to calculate half-lives ($t_{1/2}$) at 20°C (for results in DCM, see the Supplementary Materials). These are compared to the half-lives observed following 2PE in MeCN. 2PA cross sections (σ_2) of stable isomers were measured in toluene by an open-aperture Z-scan technique at 800-nm wavelength. Details of each measurement are given in the Supplementary Materials.

	$\varphi_{s\rightarrow m}$ (%)	$\varphi_{m\rightarrow s}$ (%)	$\Delta^{\ddagger}G°$ (kJ mol^{-1})*	$t_{1/2}$ (20°C) (min)*	$t_{1/2}$ (min)†	σ_2 (GM)
1	15.1 ± 0.3	5.0 ± 0.1	86.2 ± 0.1	4.35 ± 0.12	2.8 ± 0.3	260 ± 40
2	5.2 ± 0.1	1.59 ± 0.01	87.1 ± 0.1	6.15 ± 0.17	4.1 ± 0.1	200 ± 20
3	2.3 ± 0.1	0.86 ± 0.04	87.8 ± 0.1	8.47 ± 0.08	6.0 ± 0.1	1100 ± 400
Motor core	14‡	50‡	85§	3.17§	–	<5

*From Eyring analysis (section S5.3). †From the time evolution of ΔOD spectra after 2PE. The ambient temperature during the ΔOD spectroscopy measurement was stable at ~23°C. ‡Value previously reported in the literature with toluene as solvent (*38*). §Value previously reported in the literature with hexane as solvent (*47*).

in MeCN were recorded before and after irradiation with an 800-nm femtosecond laser. Figure 2B shows difference absorption (ΔOD) spectra calculated by subtracting the spectrum before irradiation from the spectrum after irradiation. These spectra show bathochromic shifts similar to those observed under one-photon irradiation with LED light (Fig. 2A). Quadratic dependences of ΔOD on the incident light intensity demonstrate the characteristic 2PA process (section S6.2). Upon removing the light source and keeping the samples in the dark, the spectra reverted to the original ones within time frames consistent with Eyring analysis (Table 1). Moreover, over the course of several consecutive irradiation cycles using 2PA, no substantial (**1** and **2**) or only small (**3**) deviations in the ΔOD spectra of these motors were observed (inset in Fig. 2B and fig. S30), indicating the remarkable photostability of these motors. Therefore, we conclude that the rotation of these motors can be driven using 800-nm light.

The σ_2 values measured by an open-aperture Z-scan technique (*48*, *49*) (section S7) are several orders of magnitude higher than that of the bare motor core (Table 1). They are also comparable to an efficient 2PA dye, AF-343 (σ_2 ~ 1000 GM), which has been previously used as an antenna to power molecular motors (*22*). The large σ_2 opens prospects in applications where the use of low-intensity NIR light and three-dimensional localization is essential (e.g., biological systems and soft materials).

PL properties of $\mathbf{1_s}$

Figure 3A shows a time-resolved PL map of $\mathbf{1_s}$ in MeCN under 1PE at 445 nm, which lies on the lowest-energy absorption peak of $\mathbf{1_s}$. The PL map displays a short-lived PL, which decays with a ~15-ps lifetime (Fig. 3D). Within the same time, PL undergoes a distinct red shift (white line), which is assigned to wave packet motion from the FC region toward the CI. This result is in line with previous studies of second-generation molecular motors (*37*, *38*) where the short-lived PL competes with fast S_1 excited-state relaxation, which leads to nonradiative photoisomerization. Therefore, motor **1** exhibits only its rotation function under 445-nm excitation. The extremely low quantum yields of ~10^{-4} to 10^{-3} of this PL (*37*, *39*) make it impossible for it to be used in PL-based localization measurements.

When the excitation wavelength is shifted to 400 nm (Fig. 3B), a new long-lived (lifetime of ~1.6 ns; Fig. 3D) PL is observed in the 420- to 500-nm region, in addition to the before-mentioned short-lived PL. The intensity of the former is about two orders of magnitude higher compared to the latter (fig. S32) so that the long-lived PL can be used for localizing molecular motors; the onset of dual-function selection lies in the 435- to 440-nm region (section S8.2). Note that we carefully ruled out PL from possible contaminations (section S3), molecular aggregation (section S8.2), or $\mathbf{1_m}$ isomers (section S10).

At long times, the long-lived PL outcompetes the short-lived one, which results in a blue shift of the mean wavelength (Fig. 3B). A similar argument is also applicable to the blue shift of the mean wavelength at times longer than 50 ps of **1** under 445-nm excitation, but there, the long-lived PL has a much lower amplitude and therefore is hardly visible in the PL map (fig. S37).

The PL map under 2PE at 800 nm (Fig. 3C) is similar to the one under 1PE at 445 nm (Fig. 3A), and thus, motor **1** exhibits only its rotation function under NIR light. This offers another exciting approach for switching between motor rotation and PL, e.g., by inserting/removing a second harmonic generator into the NIR beam. Ultrafast TA experiments confirmed the aforementioned excited-state dynamics and provided evidence for subsequent formation of the photogenerated metastable isomer $\mathbf{1_m}$ (see Supplementary Materials, section S11).

On the basis of our experimental results, we propose the long-lived PL of motor **1** to originate from a high-lying minimum on the S_1 surface populated via initial excitation to S_2 followed by IC. Direct emission from S_2, while possible in principle, is unlikely given the relatively small energy gap between the two excited states (see section S12) and the partially flexible nature of **1** favoring ultrafast nonradiative relaxation.

DISCUSSION

In the case of motor **1**, the addition of one triphenylamine substituent was enough to give this compound a PL signal in addition to its function as a motor, and a large σ_2. This leaves open the possibility for further functionalization of **1**, especially in the lower half. Motor **3** behaves very similarly to **1**, also allowing for tuning the selectivity between the motor rotation and PL function by using different excitation wavelengths. Furthermore, motor **3** has two important advantages: (i) the absorption spectrum is red-shifted (the formation of $\mathbf{3_m}$ was observed up to an excitation wavelength of 565 nm, which is among the longest wavelengths reported to date for directly powering an artificial rotary molecular motor), and (ii) the σ_2 of $\mathbf{3_s}$ is larger by a factor of 4 compared to that of $\mathbf{1_s}$. However, these are counterbalanced by the larger size of **3**, its lower stability (sections S6.2 and S6.4), and the more restricted possibilities for further functionalization.

In contrast to motors **1** and **3**, **2** exhibits little selectivity between the motor rotation and PL upon changing the excitation wavelength. TD-DFT simulations shed some light on this observation: The energy difference between the electronic transitions to S_1 and S_2 becomes negligible in the case of $\mathbf{2_s}$, making these states almost degenerate (see section S12). Therefore, the long-lived PL observable in $\mathbf{2_s}$ independently of the excitation wavelength is a consequence of the near proximity of S_1 and S_2 in $\mathbf{2_s}$ and therefore the impossibility to selectively excite either of them. This finding reinforces our claim that population of a local minimum on S_1 via relaxation from S_2 is the origin of the long-lived PL. The presence of long-lived PL following 2PE of **2**, which is absent for **1** and **3**, can be rationalized assuming only S_1 to be accessible via this excitation pathway.

In summary, we present the first set of artificial molecular motors displaying dual function of rotation and long-lived PL. The properties of our newly described motors make them uniquely attractive for any kind of application where it is required to alternate

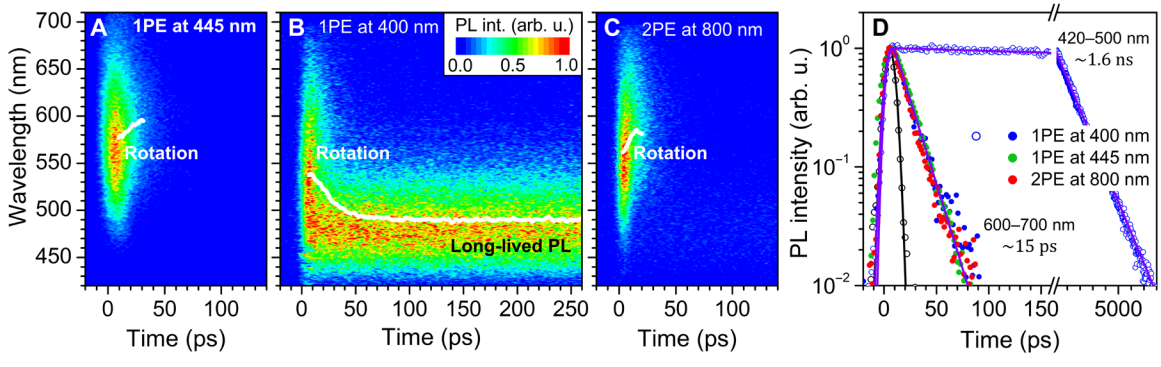

Fig. 3. Time-resolved PL properties of motor 1. (**A** to **C**) Time-resolved PL maps of $\mathbf{1_s}$ under 1PE at 445 nm (A) and 400 nm (B), as well as 2PE at 800 nm (C). The white lines show the mean wavelengths calculated as $\int \lambda S(\lambda, t)d\lambda / \int S(\lambda, t)d\lambda$ of spectral slices $S(\lambda, t)$ at a particular time t of the PL maps (the region of 10% of maximum PL intensity was selected as at lower intensities the mean wavelength becomes too noisy). The mean wavelengths (energies) and PL maps with a longer time scale as well as those for motors **2** and **3** are available in section S9. (**D**) PL transients (dots) of $\mathbf{1_s}$ integrated over different wavelength regions under 400 nm (blue) and 445 nm (green) 1PEs as well as 800 nm 2PE (red). The solid lines show the best fits to a single-exponential function convoluted to the apparatus function (black). The molar concentration of $\mathbf{1_s}$ was set to 1.0×10^{-5} M with MeCN as the solvent. The peak intensities were ~0.5 MW cm^{-2} for 400- and 445-nm excitations and ~1 GW cm^{-2} for 800-nm excitation.

between motor rotation and PL in situ. We foresee especially broad applicability in biological studies, where it is key to obtain the distribution and positioning of a molecular machine before and/or after initiating its operation while not compromising the possibility to use low-intensity NIR light for its operation.

MATERIALS AND METHODS

Preparation and characterization of compounds

Reagents were purchased from Sigma-Aldrich, Acros, or TCI Europe and were used as received. Solvents were reagent grade and used without prior water removal unless otherwise indicated. Anhydrous solvents were obtained from an MBraun SPS-800 solvent purification system or directly bought from Acros. Solvents were degassed by purging with N_2 for a minimum of 30 min or by conducting three freeze-pump-thaw cycles.

Flash column chromatography was performed on silica gel (Merck, type 9385, 230 to 400 mesh) or on a Büchi Reveleris purification system using Büchi silica cartridges. Thin-layer chromatography was carried out on aluminum sheets coated with silica gel 60 F254 (Merck). Compounds were visualized with a UV lamp and/or by staining with $KMnO_4$, ceric ammonium molybdate (CAM), or vanillin.

9-Diazo-9*H*-fluorene (**S3**) (*50*) and the unsubstituted motor (*47*) were prepared according to known and previously reported procedures. Stable and metastable isomers are denominated with a subscript "s" or "m," respectively.

^{1}H and ^{13}C NMR spectra were recorded on a Varian Mercury-Plus 400 or a Bruker Avance 600 NMR spectrometer at 298 K unless otherwise indicated. PSS studies were performed on a Varian Unity Plus 500 NMR spectrometer. Chemical shifts are given in parts per million relative to the residual solvent signal. Multiplets in ^{1}H NMR spectra are designated as follows: s (singlet), d (doublet), t (triplet), q (quartet), p (pentet), m (multiplet), and br (broad). High-resolution mass spectrometry was performed on an LTQ Orbitrap XL spectrometer. Steady-state ultraviolet-visible (UV-vis) absorption spectra were recorded on a Lambda900 UV-vis-NIR spectrometer, an Agilent 8453 UV-vis Diode Array System, or a Specord S600 spectrophotometer, equipped with Quantum Northwest Peltier controllers, in 10-mm quartz cuvettes. Irradiation experiments were performed using fiber-coupled LEDs (M420F2, M455F1, M470F3, and M565F3) obtained from Thorlabs Inc.

Difference absorption spectroscopy

Difference absorption spectroscopy measurements were performed using a UV-vis-NIR spectrometer (Lambda 900) and an amplified mode-locked Ti:sapphire laser (Legend Elite Duo, Coherent) centered at 800 nm with a 1-kHz repetition rate. The output light source of the laser beam (8 mm in diameter) irradiated a 1-cm quartz cuvette, containing the studied compounds dissolved in MeCN, with 15-min irradiation time.

For intensity-dependent experiments with two-photon irradiation at 800 nm, the peak irradiation intensity was varied between 0.45 and 4.5 GW cm^{-2}, which corresponds to an energy density between 0.1 and 1 mJ cm^{-2}. For time-evolution experiments, the irradiation intensity was set at the highest value where no photodegradation was observed. The absorption of the samples was recorded before irradiation and starting from 10 s after irradiation at different periods of time up to 1 hour; all measurements were performed in the dark. Last, difference absorption (ΔOD) spectra were obtained by subtracting the absorption spectra before irradiation from the corresponding spectra after irradiation. As the ΔOD spectra are extremely sensitive to temperature, it was maintained at ~23°C for all measurements.

For fatigue studies, samples were irradiated with peak intensities of 4.5 GW cm^{-2} for motors **1** and **2**, and 1.4 GW cm^{-2} for motor **3**, for the ΔOD dependence to be in the quadratic-dependence regime. To obtain as many irradiation cycles as possible, the irradiation time was reduced to 5 min. The absorption of the samples was recorded before and after (10-s delay) irradiation (of every cycle) so that the ΔOD spectrum was obtained. To ensure that metastable isomers of the motors proceeded completely to the second identical stable isomers, the samples were stored in the dark for at least 40 min before starting a new cycle.

Steady-state PL spectroscopies

Steady-state PL and PL excitation spectroscopies were performed using a luminescence spectrometer (Perkin Elmer LS-50B). The studied compounds were dissolved in MeCN in quartz cuvettes with an optical path length of 1 cm. Two different sets of samples with low and high concentrations (~1.0×10^{-6} and ~1.0×10^{-5} M, respectively) were prepared. By measuring both samples, PL reabsorption effects can be minimized in the low-concentration samples and weak signals of the low-energy PL bands can be recorded in the high-concentration samples. The optical densities (ODs) at the lowest-energy absorption peaks of the samples of motors **1**, **2,** and **3** with the low concentration were determined as 0.08, 0.1, and 0.11, respectively. For the samples with high concentrations, the corresponding OD values were ca. 10-fold higher than those of the low-concentration samples. To remove any unwanted artifacts (e.g., second-order diffraction of grating), PL and PL excitation spectra of pure MeCN under identical conditions were subtracted from those of the samples with studied compounds.

Time-resolved PL spectroscopy

Time-resolved PL spectroscopy measurements were carried out using a Hamamatsu C5680 streak camera equipped with a Ti:sapphire laser (Mira 900, Coherent) with a repetition rate of 76 MHz. For measurements with a time window above 2 ns, the repetition rate was lowered to 2 MHz by a pulse picker. The 800-nm beam was obtained directly from the laser output, whereas excitation wavelengths of 380, 400, and 445 nm were obtained using a second harmonic generator, and an excitation wavelength of 278 nm was obtained using a third harmonic generator. The excitation beam was focused by lenses with a 7.6-cm focal length (a 3.5-cm focal length for 800-nm excitation) into a 1-mm quartz cuvette, containing the studied compounds dissolved in MeCN. The size of the illumination spots was determined using knife-edge measurements as ~135 and ~45 μm in diameter for 400- and 800-nm excitation, respectively. For the repetition-rate dependence experiments, a 0.2-mm flow cell (Starna Scientific Ltd.) connected to a peristaltic pump (Masterflex, Cole-Parmer) to refresh the sample in the excitation spot was used, and the repetition rate of the laser was lowered to 9 kHz by a pulse picker. The apparatus functions of the setup were ~4, ~5, and ~3 ps (SDs of a Gaussian function) for the excitation wavelengths of 400, 445, and 800 nm, respectively. The peak intensities did not exceed 1 and 2 GW cm^{-2} for 400- and 800-nm excitation, respectively.

The ODs at the lowest-energy peak of samples of motors **1**, **2**, and **3** were set at 0.08, 0.1, and 0.11, respectively, so that the PL reabsorption

effect was minimized. The PL signal was collected at a ~90° angle with respect to the excitation laser beam. The polarizations of the excitation and PL channels (by placing two polarizers into these beams) were set at the magic angle (~54.7°). A band-pass filter (Thorlabs Inc., 420 to 700-nm transmission region) at the polychromator entrance slit was used to remove stray light from the excitation beams at 380, 400, and 800 nm. Meanwhile, for 278- and 445-nm excitations, long-pass filters (Thorlabs Inc.) with a cutoff wavelength of 320 and 455 nm, respectively, were used instead. Last, the PL intensity of the samples was recorded as a function of the wavelength and delay time, producing a PL map. In all measurements, room temperature was maintained at 20°C. Under excitation at 380, 400, and 445 nm with high peak intensities (>0.35 MW cm^{-2}), additional signals near zero-delay time were observed and identified as Raman lines of MeCN (fig. S1) (*51*).

TA spectroscopy

The setup for TA spectroscopy was based on a pump-probe arrangement described previously (*22*). In brief, an amplified mode-locked Ti:sapphire laser (Legend Elite Duo, Coherent) centered at 800 nm (1-kHz repetition rate) was used. The laser output was split into pump (~90%) and probe (~10%) beams. For 1PE at 400 nm, the laser output was frequency-doubled using a β-barium borate crystal. A mechanical translation stage (LS-180, Physik Instrumente) with 508-mm excursion was used to delay the probe pulse with respect to the pump pulse. The probe beam was focused into a 2-mm sapphire crystal to generate a white light (400 to 850 nm) continuum (WLC). A short-pass filter with a cutoff wavelength of 750 nm placed into the probe beam was used to remove residual fundamental frequency radiation from the WLC. The polarization of the pump and probe beams was linear and set at the magic angle (54.7°). Both the pump and the probe beams were focused and spatially overlapped in a flow cell (Starna Scientific Ltd.), connected to a peristaltic pump (Masterflex, Cole-Parmer) to refresh the sample in the excitation spot. TA of the probe beam in the flow cell was recorded using two different types of detectors, a 350- to 700-nm compact spectrometer (CCS100/M, Thorlabs Inc.) and a silicon photodiode (DET36A, Thorlabs Inc.) amplified by a lock-in amplifier (SR830 DSP, Stanford Research Systems). The spectrometer detected the TA spectra (and spectrotemporal TA maps) in the wavelength region of 400 to 700 nm; however, it had a lower signal-to-noise ratio as compared to the lock-in referenced photodiode. The photodiode detector detected TA signals at a particular probe wavelength using a band-pass filter placed in front of the photodiode. For the TA kinetic traces at 510 and 700 nm, band-pass filters with central wavelengths of 508.5 and 700 nm and full width at half maximum (FWHM) of 10 and 40 nm, respectively, were used. This arrangement improved the sensitivity down to $\Delta OD \cong 1 \times 10^{-5}$, which allowed obtaining the signals under 2PE conditions. Further details of data acquisition, correction of the zero-delay time (as a function of the probe wavelength), and solvent contribution around zero-delay time were described in a previous publication (*22*).

2PA cross-sectional measurements

2PA cross sections of the studied compounds were determined using an open-aperture Z-scan technique (for setup see fig. S3A) (*48*, *49*). The experiments were performed using an amplified mode-locked Ti:sapphire laser (Legend Elite Duo, Coherent) centered at 800 nm (1-kHz repetition rate, ~220-fs pulse duration; see fig. S3B). The output laser beam was focused by a converging lens with a focal length of 15 cm through a quartz cuvette with an optical path of 1 mm containing the studied compounds. The 1-mm cuvette satisfied the condition that the optical path length is less than the Rayleigh length of the focusing lens of ~4.8 mm. The cuvette was mounted onto a motorized translation stage (PLS-85, PI miCos GmbH) so that it could be moved back and forth along the propagation direction of the focused beam (Z-scan stage). After transmission through the cuvette, the beam was collected by a lens with a shorter focal length of 10 cm to ensure that the entire light beam was collected. A photodiode detector (LM-2 VIS, Coherent) equipped with a power meter (FieldMaster FM-0210, Coherent) was used to measure the transmitted power. A long-pass filter with a cutoff wavelength of 715 nm placed in front of the detector was used to eliminate any PL from the sample. Neutral density filters in front of the detector ensured its linear regime. The transmitted powers were measured while scanning the sample along the beam propagation direction through the focal point. Last, the transmitted powers taking the attenuation of the used neutral density filters into account at different Z positions were obtained (i.e., a Z-scan response).

To obtain the beam shape near the focal point, a knife-edge technique was performed. This was done by mounting another motorized translation stage (X-scan stage) onto the Z-scan translation stage in a perpendicular alignment to each other. A metal blade mounted onto the X-scan translation stage was scanned orthogonally to the beam propagation direction and the transmitted power was measured. By taking the first-order derivative of the transmitted power with respect to the transverse beam position X, a spatial intensity distribution in the transverse direction of the beam was obtained. The beam diameter was taken as an FWHM of the intensity distribution. The FWHM was determined from a Gaussian fitting function to the experimentally obtained intensity distribution with an SD σ (FWHM ≈ 2.355 × σ). The measurements were repeated at different Z positions so that a beam shape in the XZ plane was reconstructed (fig. S3C).

SUPPLEMENTARY MATERIALS

Supplementary material for this article is available at https://science.org/doi/10.1126/sciadv.add0410

REFERENCES AND NOTES

1. J.-P. Sauvage, From chemical topology to molecular machines (Nobel lecture). *Angew. Chem. Int. Ed.* **56**, 11080–11093 (2017).
2. C. J. Bruns, J. F. Stoddart, *The Nature of the Mechanical Bond: From Molecules to Machines* (John Wiley & Sons Inc., 2016).
3. W. R. Browne, B. L. Feringa, Making molecular machines work. *Nat. Nanotechnol.* **1**, 25–35 (2006).
4. J. P. Sauvage, P. Gaspard, *From Non-Covalent Assemblies to Molecular Machines* (Wiley-VCH Verlag GmbH & Co. KGaA, 2011).
5. C. Pezzato, C. Cheng, J. F. Stoddart, R. D. Astumian, Mastering the non-equilibrium assembly and operation of molecular machines. *Chem. Soc. Rev.* **46**, 5491–5507 (2017).
6. M. Baroncini, S. Silvi, A. Credi, Photo- and redox-driven artificial molecular motors. *Chem. Rev.* **120**, 200–268 (2020).
7. V. García-López, D. Liu, J. M. Tour, Light-activated organic molecular motors and their applications. *Chem. Rev.* **120**, 79–124 (2020).
8. S. Kassem, T. van Leeuwen, A. S. Lubbe, M. R. Wilson, B. L. Feringa, D. A. Leigh, Artificial molecular motors. *Chem. Soc. Rev.* **46**, 2592–2621 (2017).
9. F. Lancia, A. Ryabchun, N. Katsonis, Life-like motion driven by artificial molecular machines. *Nat. Rev. Chem.* **3**, 536–551 (2019).
10. N. Koumura, E. M. Geertsema, A. Meetsma, B. L. Feringa, Light-driven molecular rotor: Unidirectional rotation controlled by a single stereogenic center. *J. Am. Chem. Soc.* **122**, 12005–12006 (2000).

11. D. Roke, S. J. Wezenberg, B. L. Feringa, Molecular rotary motors: Unidirectional motion around double bonds. *Proc. Natl. Acad. Sci. U.S.A.* **115**, 9423–9431 (2018).
12. R. D. Astumian, How molecular motors work—Insights from the molecular machinist's toolbox: The Nobel prize in chemistry 2016. *Chem. Sci.* **8**, 840–845 (2017).
13. Q. Li, G. Fuks, E. Moulin, M. Maaloum, M. Rawiso, I. Kulic, J. T. Foy, N. Giuseppone, Macroscopic contraction of a gel induced by the integrated motion of light-driven molecular motors. *Nat. Nanotechnol.* **10**, 161–165 (2015).
14. J. Chen, F. K.-C. Leung, M. C. A. Stuart, T. Kajitani, T. Fukushima, E. van der Giessen, B. L. Feringa, Artificial muscle-like function from hierarchical supramolecular assembly of photoresponsive molecular motors. *Nat. Chem.* **10**, 132–138 (2017).
15. D. J. van Dijken, J. Chen, M. C. A. Stuart, L. Hou, B. L. Feringa, Amphiphilic molecular motors for responsive aggregation in water. *J. Am. Chem. Soc.* **138**, 660–669 (2016).
16. W. Danowski, T. van Leeuwen, S. Abdolahzadeh, D. Roke, W. R. Browne, S. J. Wezenberg, B. L. Feringa, Unidirectional rotary motion in a metal–organic framework. *Nat. Nanotechnol.* **14**, 488–494 (2019).
17. F. Castiglioni, W. Danowski, J. Perego, F. K. C. Leung, P. Sozzani, S. Bracco, S. J. Wezenberg, A. Comotti, B. L. Feringa, Modulation of porosity in a solid material enabled by bulk photoisomerization of an overcrowded alkene. *Nat. Chem.* **12**, 595–602 (2020).
18. Q. Zhou, J. Chen, Y. Luan, P. A. Vainikka, S. Thallmair, S. J. Marrink, B. L. Feringa, P. van Rijn, Unidirectional rotating molecular motors dynamically interact with adsorbed proteins to direct the fate of mesenchymal stem cells. *Sci. Adv.* **6**, eaay2756 (2020).
19. D. Liu, V. García-López, R. S. Gunasekera, L. Greer Nilewski, L. B. Alemany, A. Aliyan, T. Jin, G. Wang, J. M. Tour, R. Pal, Near-infrared light activates molecular nanomachines to drill into and kill cells. *ACS Nano* **13**, 6813–6823 (2019).
20. T. Kondo, W. J. Chen, G. S. Schlau-Cohen, Single-molecule fluorescence spectroscopy of photosynthetic systems. *Chem. Rev.* **117**, 860–898 (2017).
21. S. Shashkova, M. C. Leake, Single-molecule fluorescence microscopy review: Shedding new light on old problems. *Biosci. Rep.* **37**, BSR20170031 (2017).
22. L. Pfeifer, N. V. Hoang, M. Scherübl, M. S. Pshenichnikov, B. L. Feringa, Powering rotary molecular motors with low-intensity near-infrared light. *Sci. Adv.* **6**, eabb6165 (2020).
23. D. R. S. Pooler, A. S. Lubbe, S. Crespi, B. L. Feringa, Designing light-driven rotary molecular motors. *Chem. Sci.* **12**, 14964–14986 (2021).
24. B. Krajnik, J. Chen, M. A. Watson, S. L. Cockroft, B. L. Feringa, J. Hofkens, Defocused imaging of UV-driven surface-bound molecular motors. *J. Am. Chem. Soc.* **139**, 7156–7159 (2017).
25. J. Chen, J. Vachon, B. L. Feringa, Light-driven molecular motors on surfaces for single molecular imaging. *J. Vis. Exp.* , e58750 (2019).
26. T. Itoh, Fluorescence and phosphorescence from higher excited states of organic molecules. *Chem. Rev.* **112**, 4541–4568 (2012).
27. A. P. Demchenko, V. I. Tomin, P.-T. Chou, Breaking the kasha rule for more efficient photochemistry. *Chem. Rev.* **117**, 13353–13381 (2017).
28. J. C. del Valle, J. Catalán, Kasha's Rule: A reappraisal. *Phys. Chem. Chem. Phys.* **21**, 10061–10069 (2019).
29. M. Beer, H. C. Longuet-Higgins, Anomalous light emission of azulene. *J. Chem. Phys.* **23**, 1390–1391 (1955).
30. A. Janowski, J. Rzeszotarska, Anomalous (S2 → S0) luminescence of some derivatives of triphenylmethane dyes and their complexes with rare earth metals. *J. Lumin.* **21**, 409–416 (1980).
31. M. Ravikanth, D. Reddy, T. K. Chandrashekar, Fluorescence properties of distorted short-chain basket handle porphyrins. *J. Photochem. Photobiol. A* **72**, 61–67 (1993).
32. D. Chahraoui, P. Valat, J. Kossanyi, Fluorescence of phthalocyanines: Emission from an upper excited state. *Res. Chem. Intermed.* **17**, 219–232 (1992).
33. J. A. Mondal, H. N. Ghosh, T. Mukherjee, D. K. Palit, S2 fluorescence and ultrafast relaxation dynamics of the S2 and s1 states of a ketocyanine dye. *J. Phys. Chem. A* **109**, 6836–6846 (2005).
34. S. Muralidharan, A. J. Lough, K. Yates, Conformational effects on photophysical properties of selected bichromophoric anthracene derivatives. *J. Photochem. Photobiol. A* **71**, 245–255 (1993).
35. H. Song, K. Wang, Z. Kuang, Y. S. Zhao, Q. Guo, A. Xia, Solvent modulated excited state processes of push–pull molecule with hybridized local excitation and intramolecular charge transfer character. *Phys. Chem. Chem. Phys.* **21**, 3894–3902 (2019).
36. H. Qian, M. E. Cousins, E. H. Horak, A. Wakefield, M. D. Liptak, I. Aprahamian, Suppression of Kasha's rule as a mechanism for fluorescent molecular rotors and aggregation-induced emission. *Nat. Chem.* **9**, 83–87 (2017).
37. J. Conyard, K. Addison, I. A. Heisler, A. Cnossen, W. R. Browne, B. L. Feringa, S. R. Meech, Ultrafast dynamics in the power stroke of a molecular rotary motor. *Nat. Chem.* **4**, 547–551 (2012).
38. J. Conyard, A. Cnossen, W. R. Browne, B. L. Feringa, S. R. Meech, Chemically optimizing operational efficiency of molecular rotary motors. *J. Am. Chem. Soc.* **136**, 9692–9700 (2014).
39. C. R. Hall, J. Conyard, I. A. Heisler, G. Jones, J. Frost, W. R. Browne, B. L. Feringa, S. R. Meech, Ultrafast dynamics in light-driven molecular rotary motors probed by femtosecond stimulated Raman spectroscopy. *J. Am. Chem. Soc.* **139**, 7408–7414 (2017).
40. Y. Li, F. Liu, B. Wang, Q. Su, W. Wang, K. Morokuma, Different conical intersections control nonadiabatic photochemistry of fluorene light-driven molecular rotary motor: A CASSCF and spin-flip DFT study. *J. Chem. Phys.* **145**, 244311 (2016).
41. Y. Gao, Y. Qu, T. Jiang, H. Zhang, N. He, B. Li, J. Wu, J. Hua, Alkyl-triphenylamine end-capped triazines with AIE and large two-photon absorption cross-sections for bioimaging. *J. Mater. Chem. C* **2**, 6353–6361 (2014).
42. Y. Liu, M. Kong, Q. Zhang, Z. Zhang, H. Zhou, S. Zhang, S. Li, J. Wu, Y. Tian, A series of triphenylamine-based two-photon absorbing materials with AIE property for biological imaging. *J. Mater. Chem. B* **2**, 5430–5440 (2014).
43. Y. Zhang, M. Jiang, G.-C. Han, K. Zhao, B. Z. Tang, K. S. Wong, Solvent effect and two-photon optical properties of triphenylamine-based donor–acceptor fluorophores. *J. Phys. Chem. C* **119**, 27630–27638 (2015).
44. A. Kazaryan, J. C. M. Kistemaker, L. V. Schäfer, W. R. Browne, B. L. Feringa, M. Filatov, Understanding the dynamics behind the photoisomerization of a light-driven fluorene molecular rotary motor. *J. Phys. Chem. A* **114**, 5058–5067 (2010).
45. R. Beekmeyer, M. A. Parkes, L. Ridgwell, J. W. Riley, J. Chen, B. L. Feringa, A. Kerridge, H. H. Fielding, Unravelling the electronic structure and dynamics of an isolated molecular rotary motor in the gas-phase. *Chem. Sci.* **8**, 6141–6148 (2017).
46. J. Vicario, A. Meetsma, B. L. Feringa, Controlling the speed of rotation in molecular motors. Dramatic acceleration of the rotary motion by structural modification. *Chem. Commun.* 5910–5912 (2005).
47. J. Vicario, M. Walko, A. Meetsma, B. L. Feringa, Fine tuning of the rotary motion by structural modification in light-driven unidirectional molecular motors. *J. Am. Chem. Soc.* **128**, 5127–5135 (2006).
48. M. Sheik-Bahae, A. A. Said, T. H. Wei, D. J. Hagan, E. W. van Stryland, Sensitive measurement of optical nonlinearities using a single beam. *IEEE J. Quantum Electron.* **26**, 760–769 (1990).
49. P. Sengupta, J. Balaji, S. Banerjee, R. Philip, G. Ravindra Kumar, S. Maiti, Sensitive measurement of absolute two-photon absorption cross sections. *J. Chem. Phys.* **112**, 9201–9205 (2000).
50. J. Bauer, L. Hou, J. C. M. Kistemaker, B. L. Feringa, Tuning the rotation rate of light-driven molecular motors. *J. Org. Chem.* **79**, 4446–4455 (2014).
51. C. Chen, X. Huang, D. Lu, Y. Huang, B. Han, Q. Zhou, F. Li, T. Cui, High pressure Raman spectroscopy investigation on acetonitrile and acetonitrile-water mixture. *RSC Adv.* **5**, 84216–84222 (2015).
52. R. Ahmad, M. S. Rafique, A. Ajami, S. Bashir, W. Husinsky, S. Iqbal, Influence of laser and material parameters on two photon absorption in rhodamine B and rhodamine 6G solutions in MeOH. *Optik* **183**, 835–841 (2019).
53. L.-S. Tan, R. Kannan, M. J. Matuszewski, I. J. Khur, W. A. Feld, T. D. Dang, A. G. Dombroskie, R. A. Vaia, S. J. Clarson, G. S. He, T.-C. Lin, P. N. Prasad, Functionalization of heterocyclic diphenylamino-based two-photon absorbing materials for microfabrication, data storage, and upconverted imaging. *Proc. SPIE* **4797**, 171–178 (2003).
54. Z. Liu, Y. Wang, X. Zhang, Y. Xu, Y. Chen, J. Tian, Nonlinear optical properties of graphene oxide in nanosecond and picosecond regimes. *Appl. Phys. Lett.* **94**, 021902 (2009).
55. N. Liaros, J. T. Fourkas, The characterization of absorptive nonlinearities. *Laser Photonics Rev.* **11**, 1700106 (2017).
56. P. Štacko, J. C. M. Kistemaker, B. L. Feringa, Fluorine-substituted molecular motors with a quaternary stereogenic center. *Chem. A Eur. J.* **23**, 6643–6653 (2017).
57. J. Conyard, P. Stacko, J. Chen, S. McDonagh, C. R. Hall, S. P. Laptenok, W. R. Browne, B. L. Feringa, S. R. Meech, Ultrafast excited state dynamics in molecular motors: Coupling of motor length to medium viscosity. *J. Phys. Chem. A* **121**, 2138–2150 (2017).
58. D. Roke, C. Stuckhardt, W. Danowski, S. J. Wezenberg, B. L. Feringa, Light-gated rotation in a molecular motor functionalized with a dithienylethene switch. *Angew. Chem. Int. Ed.* **57**, 10515–10519 (2018).
59. J. Chen, K.-Y. Chen, G. T. Carroll, B. L. Feringa, Facile assembly of light-driven molecular motors onto a solid surface. *Chem. Commun.* **50**, 12641–12644 (2014).
60. L. Pfeifer, M. Scherübl, M. Fellert, W. Danowski, J. Cheng, J. Pol, B. L. Feringa, Photoefficient 2nd generation molecular motors responsive to visible light. *Chem. Sci.* **10**, 8768–8773 (2019).
61. H. J. Kuhn, S. E. Braslavsky, R. Schmidt, Chemical actinometry (IUPAC technical report). *Pure Appl. Chem.* **76**, 2105–2146 (2004).
62. B. Gu, Y. X. Fan, J. Chen, H. T. Wang, J. He, W. Ji, Z-scan theory of two-photon absorption saturation and experimental evidence. *J. Appl. Phys.* **102**, 083101 (2007).
63. Y. Hong, J. W. Y. Lam, B. Z. Tang, Aggregation-induced emission. *Chem. Soc. Rev.* **40**, 5361–5388 (2011).
64. Y. Li, H. Lin, C. Luo, Y. Wang, C. Jiang, R. Qi, R. Huang, J. Travas-Sejdic, H. Peng, Aggregation induced red shift emission of phosphorus doped carbon dots. *RSC Adv.* **7**, 32225–32228 (2017).
65. C. Katan, F. Terenziani, O. Mongin, M. H. V. Werts, L. Porrès, T. Pons, J. Mertz, S. Tretiak, M. Blanchard-Desce, Effects of (multi)branching of dipolar chromophores on photophysical properties and two-photon absorption. *J. Phys. Chem. A* **109**, 3024–3037 (2005).

66. S. Lee, D. Kim, Symmetry-dependent intramolecular charge transfer dynamics of pyrene derivatives investigated by two-photon excitation. *J. Phys. Chem. A* **120**, 9217–9223 (2016).
67. M. Byrdin, V. Thiagarajan, S. Villette, A. Espagne, K. Brettel, Use of ruthenium dyes for subnanosecond detector fidelity testing in real time transient absorption. *Rev. Sci. Instrum.* **80**, 043102 (2009).
68. P. Parkinson, D. V. Kondratuk, C. Menelaou, J. Q. Gong, H. L. Anderson, L. M. Herz, Chromophores in molecular nanorings: When is a ring a ring? *J. Phys. Chem. Lett.* **5**, 4356–4361 (2014).
69. J. R. Lakowicz, *Principles of Fluorescence Spectroscopy* (Springer, 2006).
70. P. Pracht, F. Bohle, S. Grimme, Automated exploration of the low-energy chemical space with fast quantum chemical methods. *Phys. Chem. Chem. Phys.* **22**, 7169–7192 (2020).
71. M. J. Frisch, G. W. Trucks, H. B. Schlegel, G. E. Scuseria, M. A. Robb, J. R. Cheeseman, G. Scalmani, V. Barone, G. A. Petersson, H. Nakatsuji, X. Li, M. Caricato, A. v. Marenich, J. Bloino, B. G. Janesko, R. Gomperts, B. Mennucci, H. P. Hratchian, J. v. Ortiz, A. F. Izmaylov, J. L. Sonnenberg, D. Williams-Young, F. Ding, F. Lipparini, F. Egidi, J. Goings, B. Peng, A. Petrone, T. Henderson, D. Ranasinghe, V. G. Zakrzewski, J. Gao, N. Rega, G. Zheng, W. Liang, M. Hada, M. Ehara, K. Toyota, R. Fukuda, J. Hasegawa, M. Ishida, T. Nakajima, Y. Honda, O. Kitao, H. Nakai, T. Vreven, K. Throssell, J. A. Montgomery Jr., J. E. Peralta, F. Ogliaro, M. J. Bearpark, J. J. Heyd, E. N. Brothers, K. N. Kudin, V. N. Staroverov, T. A. Keith, R. Kobayashi, J. Normand, K. Raghavachari, A. P. Rendell, J. C. Burant, S. S. Iyengar, J. Tomasi, M. Cossi, J. M. Millam, M. Klene, C. Adamo, R. Cammi, J. W. Ochterski, R. L. Martin, K. Morokuma, O. Farkas, J. B. Foresman, D. J. Fox, *Gaussian 16, Revision B.01* (Gaussian Inc., 2016).

Acknowledgments
Funding: This work was supported by The Netherlands Organization for Scientific Research (B.L.F.); The Royal Netherlands Academy of Arts and Sciences (B.L.F.); Dutch Ministry of Education, Culture, and Science Gravitation Program 024.001.035 (B.L.F.); European Research Council Advanced Investigator Grant 694345 (B.L.F.); European Commission Marie Skłodowska-Curie Actions Individual Fellowship 793082 (L.P.); European Commission Marie Skłodowska-Curie Actions Individual Fellowship 838280 (S.C.); and the University of Groningen. **Author contributions:** Conceptualization: L.P. and B.L.F. Data curation: L.P., N.V.H., and S.C. Formal analysis: L.P., N.V.H., and S.C. Funding acquisition: L.P., S.C., M.S.P., and B.L.F. Investigation: L.P., N.V.H., and S.C. Methodology: L.P., N.V.H., S.C., and M.S.P. Project administration: L.P., M.S.P., and B.L.F. Resources: M.S.P. and B.L.F. Supervision: M.S.P. and B.L.F. Visualization: L.P., N.V.H., and S.C. Writing—original draft: L.P., N.V.H., S.C., and M.S.P. Writing—review and editing: L.P., N.V.H., S.C., M.S.P., and B.L.F. **Competing interests:** The authors declare that they have no competing interests. **Data and materials availability:** All data needed to evaluate the conclusions in the paper are present in the paper and/or the Supplementary Materials.

Submitted 17 May 2022
Accepted 19 September 2022
Published 4 November 2022
10.1126/sciadv.add0410

ScienceAdvances

Dual-function artificial molecular motors performing rotation and photoluminescence

Lukas PfeiferNong V. HoangStefano CrespiMaxim S. PshenichnikovBen L. Feringa

Sci. Adv., 8 (44), eadd0410. • DOI: 10.1126/sciadv.add0410

Science Advances (ISSN) is published by the American Association for the Advancement of Science. 1200 New York Avenue NW, Washington, DC 20005. The title *Science Advances* is a registered trademark of AAAS.